Engineering Failure Analysis 135 (2022) 106155

Contents lists available at ScienceDirect

Engineering Failure Analysis

journal homepage: www.elsevier.com/locate/engfailanal

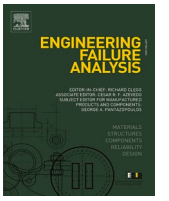

Identification of driving out force of shaft towards preventing coming out failure of shaft in shrink-fitted ceramic sleeve roll

Guowei Zhang [a], Nao-Aki Noda [b,*], Yoshikazu Sano [b], Yasushi Takase [b]

[a] *Institute of Magnetic Levitation and Electromagnetic Propulsion, China Aerospace Science and Industry Corporation Third Academy, Beijing 100143, China*

[b] *Mechanical Engineering Department, Kyushu Institute of Technology, Kitakyushu 804-8550, Japan*

ARTICLE INFO

Keywords:
Shrink-fitted ceramic sleeve roll
Driving out force
Coming out failure
Design factors
3D numerical simulation

ABSTRACT

Ceramics rolls/rollers recently developed can be used efficiently in steel manufacturing industries to produce high-quality steel plates under high temperature. However, sometimes the shrink-fitted shaft is coming out from the ceramic sleeve during the use even though no external force is applied in the coming out direction. In the previous studies, to realize the phenomena under a large number of roll rotations, numerical simulations were performed by using two-dimensional modelling. Towards preventing the failure, this paper focuses on identifying the driving out force by applying 3D numerical simulation. Here, the driving out force can be defined as the contact force appearing at a ball-stopper designed to prevent the coming out. The results show that the summation of frictional shear stress along the shrink-fitted surface is in good agreement with the driving out force. As the most fundamental design factors, the friction coefficients, the shrink fitting ratios, the shrink fitting length, and the Young's modulus of the shaft are focused. Then, those effects on the driving out force are discussed towards preventing the coming out failure.

1. Introduction

In steel manufacturing industries, a lot of rolls/rollers are used in severely corrosive atmosphere. Ceramic sleeve rolls/rollers have been developed to be used efficiently because of their high abrasion and corrosion resistance. For example, Fig. 1(a) shows the all-ceramic sink roll used in molten zinc bath whose temperature is 480℃ in continuous galvanizing lines (CGLs) [1–3]. This roll has been developed as an academic-industrial collaboration verifying that it can be used for more than ten times longer than the conventional stainless steel rolls. The all-ceramic roll consists of four parts of ceramic sleeve, three ceramic inner rings and two ceramic shafts, all of which are connected by shrink-fitting [1]. The all-ceramic roll is suitable for mass production of high quality galvanized steel sheets; and therefore, many uses can be expected in the future although the current production volume is stagnant. Fig. 1(b) illustrates the heating furnace roll used under temperature higher than 1000℃. Although the conventional stainless steel roll with ceramic coating is cooled by water circulation, the thermal expansion coefficient difference causes the surface failure such as wearing, cracking, peeling [4–9]. Since the newly roller in Fig. 1(b) has an all-ceramic sleeve connected with the hollow steel shaft by shrink fitting, the wear resistance and the bonding strength can be improved significantly. Moreover, air cooling instead of water cooling may reduce the energy loss and the maintenance cost [10–14].

It should be noted that the shrink fitting is used for the ceramic sleeve roll in Fig. 1 (a), (b) as the most suitable connection method.

* Corresponding author.
E-mail address: noda.naoaki844@mail.kyutech.jp (N.-A. Noda).

https://doi.org/10.1016/j.engfailanal.2022.106155
Received 11 November 2021; Received in revised form 23 January 2022; Accepted 12 February 2022
Available online 16 February 2022

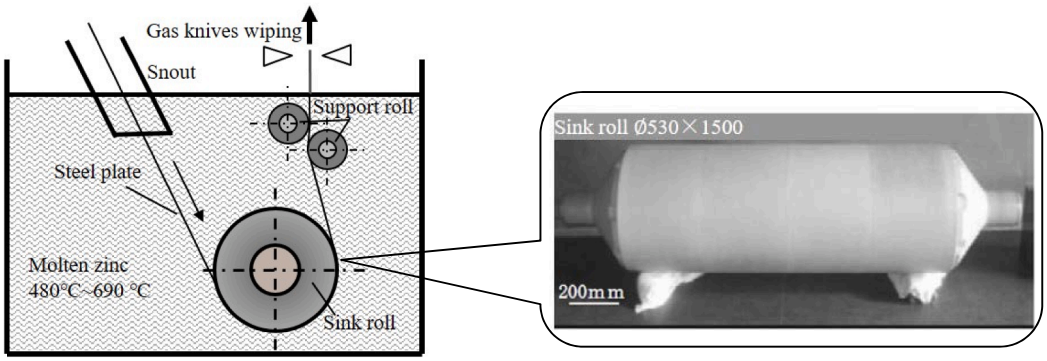

(a) All-ceramic sink roll used in molten zinc bath

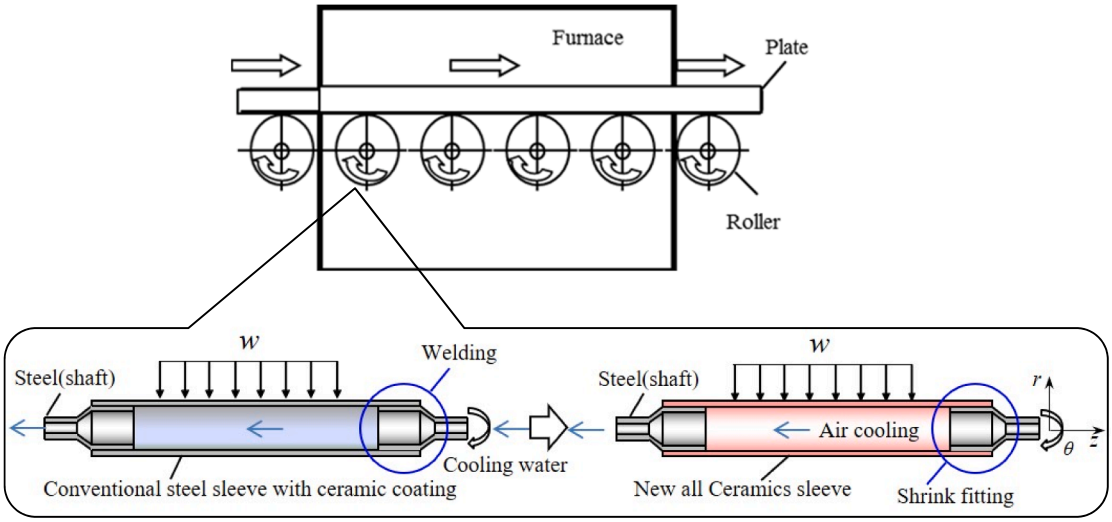

(b) Ceramic sleeve roll used in heating furnace

Fig. 1. Illustration of ceramic rolls used in steel industries.

In the previous studies, therefore, the static strength and fatigue strength of the shrink fitted portions were studied [2,3,15–17]. Also, how to reduce the hoop stress in ceramic sleeve was investigated since the thermal expansion of the steel shaft is larger than the one of the ceramic sleeve [18,19]. Regarding the CGL line, how to reduce the thermal stress was investigated when all ceramic roll is dipping into the molten metal [3,18–22]. For the maintenance of all ceramic roll, the separation condition of the sleeve and the shaft was clarified by heating the sleeve from outside [4,23,24]. In this way, several peculiar problems for ceramic sleeve roll were treated.

In this paper, a new failure of the coming out of the shaft will be considered. This is because sometimes the shrink-fitted shaft is coming out although no external force is applied in the axial direction in Fig. 1 (a). Here, the coming out direction can be defined as the axial direction indicated in the z-direction in Fig. 1 (b). This paper will focus on identifying the driving out force by applying 3D numerical simulation. Here, the driving out force can be defined as the contact force appearing at a ball-stopper designed to prevent the coming out. Towards preventing the failure, the effect of several design factors on the driving out force will be discussed. In this paper, the ball-stopper will be designed to obtain the driving force accurately and conveniently. On the basis of the present results, the real stopper can be designed in further studies to avoid the coming out phenomenon.

2. Previous studies for the coming out/slipping failure of the shrink-fitted structure

In ceramic sleeve rolls, the shrink fitting is the most suitable connection but only a small shrink fitting ratio can be applied because of the ceramic sleeve's brittleness. Previously, regarding other shrink-fitted structures, similar problems of the shaft coming out were treated. For example, the micro-slipping problem between the gear hub and shaft was investigated by Booker and Truman [25], contact separation failure for rotating thermos-elastoplastic shrink-fitted assembly was analyzed by Antony [26] and the influence of radial interference on torque capacity of the shrink-fit camshaft was studied through finite element method by Zhao and Wang et al. [27]. After the all-ceramic roll was developed, this new failure of the shaft coming out is known to appear in the ceramic sleeve rolls.

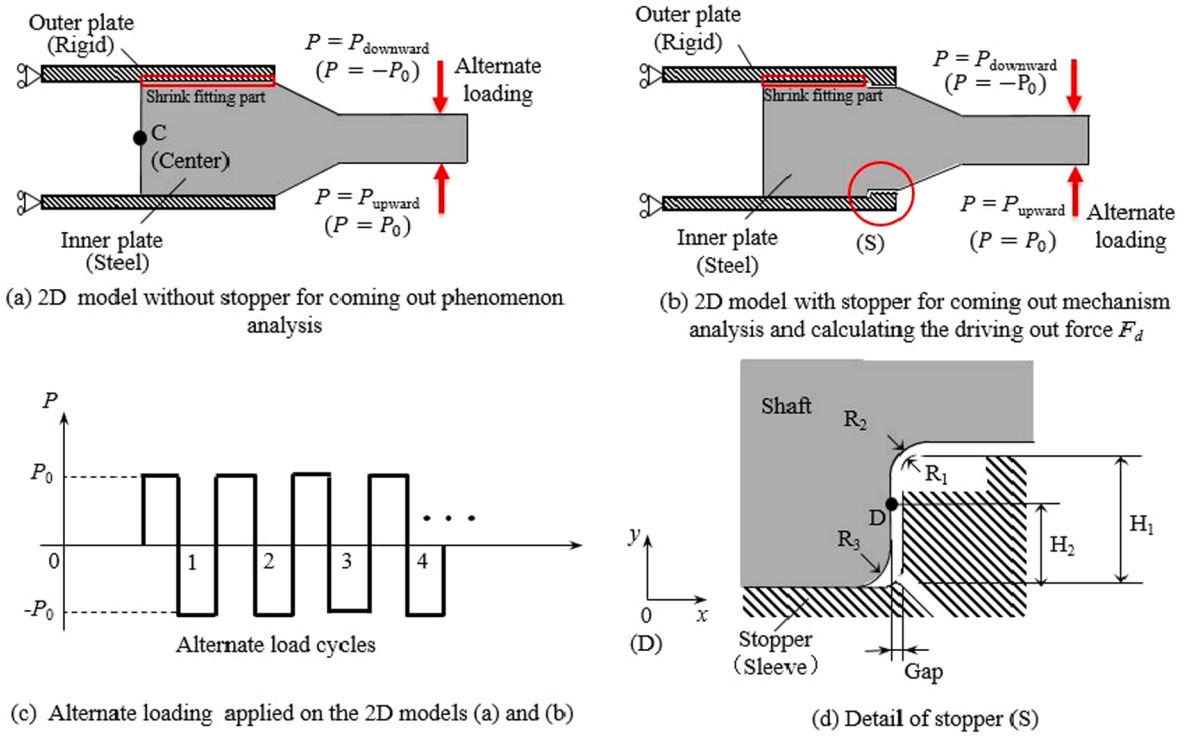

Fig. 2. Simplified 2D models (a) 2D model without stopper (b) 2D model with stopper considered in the previous paper [25,26]

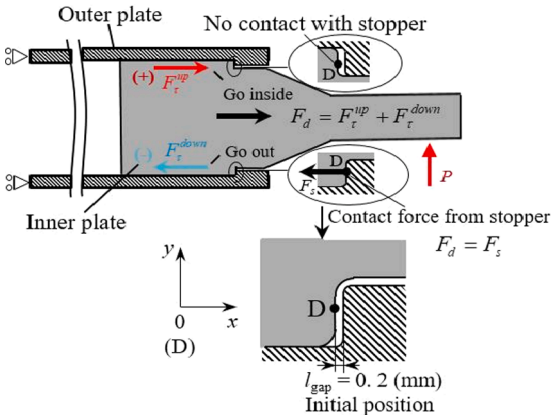

Fig. 3. The driving out force F_d can be regarded as the reaction force F_s appearing at the stopper in 2D modelling [28]

To clarify the shaft coming out phenomena, the authors have conducted several studies [13,14,19,28–30]. The coming out simulations are performed by using the finite element method that can be regarded as one of the most used numerical modeling techniques. In the first place [13,19], the coming out of the steel shaft was realized by the load shifting method where the roll rotation is replaced by the load shifting on the fixed all-ceramics roll in Fig. 1(b). Then, under which the condition the coming out appears was discussed by changing the shrink fitting ratio, the shaft Young's modulus, the friction coefficient and the magnitude of the load. To clarify the effect of such fundamental design factors under a large number of loading cycles, the numerical simulation was conducted by using the simplified two-dimensional model in Fig. 2(a). This is because the three-dimensional modelling in Fig. 1(b) needs a large calculation time to express several cycles. The two-dimensional simulation showed that the coming out behavior can be realized under a large number of alternate loading cycles efficiently [14]. By using 2D modelling with a stopper as shown in Fig. 2(b), the coming out mechanism was discussed by Zhang et.al [28 ~ 30]. Fig. 3 shows that the contact force at the stopper is regarded as the driving out force F_d. Through identifying the driving out force in this model, the generation mechanism was discussed under a large number of alternate loading. Since alternate loading is used in 2D modelling, however, the real roll rotation in 3D modelling may cause some difference of the results.

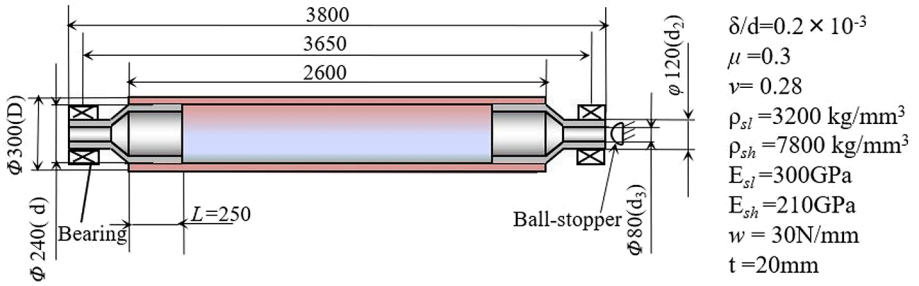

Fig. 4. Three dimensional model with standard dimensions considered in this paper (mm).

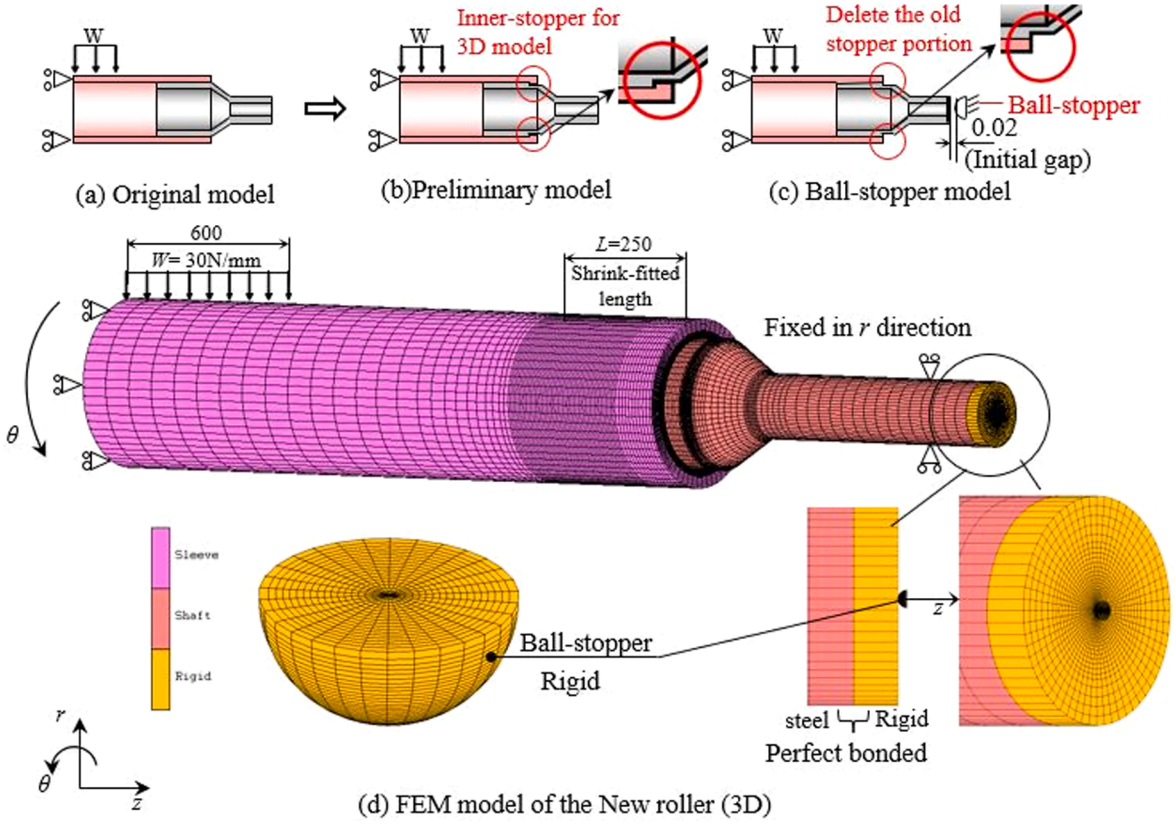

Fig. 5. Three-dimensional FEM half model having a ball-stopper to identify the driving out force F_d^{3D}

In this paper, the driving out force F_d^{3D} in the real roll will be identified. Fig. 4 illustrates the dimensions of the three-dimensional model for roll rotation used in the analysis. Here, the shrink fitting ratio is defined as δ/d, where δ is the diameter difference, d is the inner diameter of the sleeve d = 240 mm [13] and t = 20 mm is the shaft thickness. To obtain the driving force F_d^{3D}, the 3D model in Fig. 4 includes a ball-stopper whose reaction can be regarded as the driving out force F_d^{3D}. Then, by varying fundamental design factors such as the friction coefficients μ, the shrink fitting ratios δ/d, etc., the driving out force as well as the coming out displacement will be clarified in this paper. On the basis of the present results, to avoid the coming out phenomenon, the detailed design can be discussed in further studies.

3. Methodology

In this section, the analysis method how to identify the driving out force F_d^{3D} is described in detail. Fig. 5 illustrates several 3D models considered. Fig. 5(a) shows the 3D model previously used [13]. In this study, first, the inner-stopper in Fig. 5 **(b)** is considered in a similar way to the 2D model [28 ~ 30]. However, in this preliminary study, it is found that the inner-stopper in Fig. 5(b) is not suitable for the 3D modeling because of the contact position change in the circumferential direction. Therefore, as shown in Fig. 5(c), a

Table 1
Material properties of the three-dimensional model.

	Sleeve	Shaft	3D ball-stopper & Right edge of the Shaft
Material	Ceramic	Steel	Rigid
Young's modulus [GPa]	300	210	∞
Poisson's ratio	0.28	0.3	–
Tensile strength [MPa]	500	600	–
Mass density [kg/m^3]	3200	7800	–
Thermal expansion coefficient[1/K]	0.3×10^{-5}	1.2×10^{-5}	–

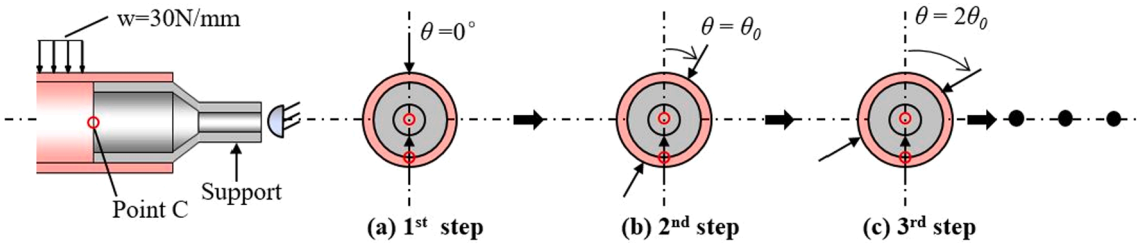

Fig. 6. Load shifting method for the new 3D model with a ball-stopper

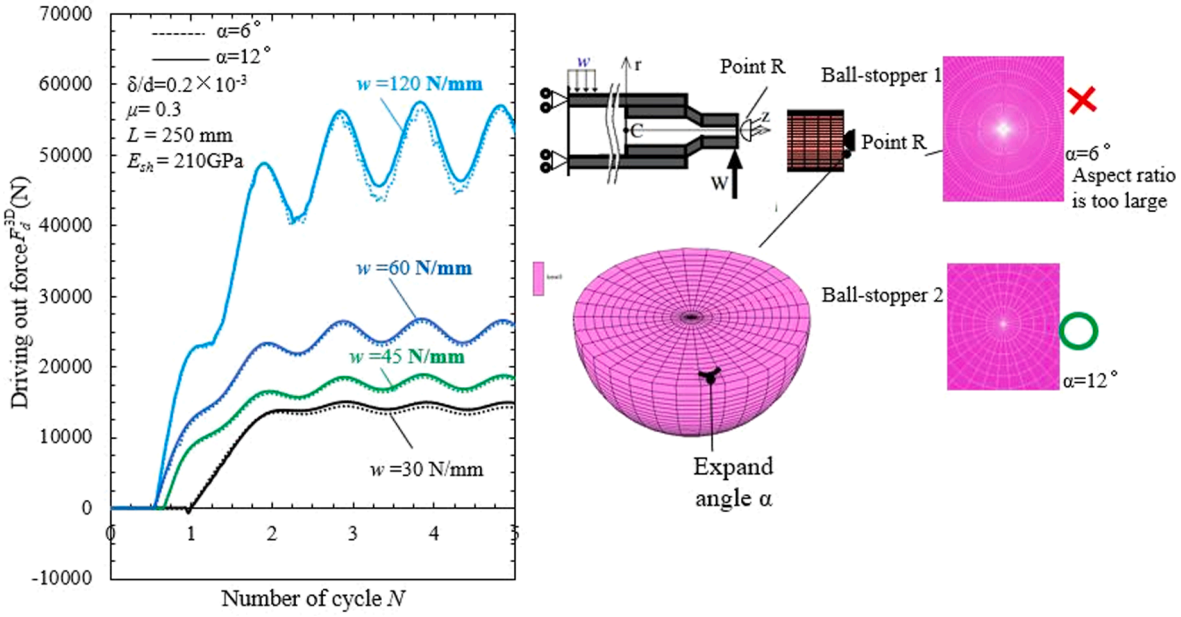

Fig. 7. Driving out force F_d^{3D} vs loading cycles N when w = 30, 45, 60, 120 N/mm under fixed μ = 0.3, δ/d = 0.2×10^{-3}, δ/d = 0.2×10^{-3}, L = 250 mm, E_{sh} = 210GPa

Table 2
Driving out force F_d^{3D} and the frictional shear force $F_\tau^{resultant}$ at $N = 3.9$ where F_d^{3D} becomes stable at the peak position when w = 30, 45, 60, 120 N/mm under fixed μ = 0.3, δ/d = 0.2×10^{-3}, L = 250 mm, E_{sh} = 210GPa.

Load w	F_d^{3D} [kN]	$F_\tau^{resultant}$ [kN]	Error
w = 30 N/mm	14.9	13.6	9.0%
w = 45 N/mm	18.8	17.2	8.2%
w = 60 N/mm	26.3	24.8	5.9%
w = 120 N/mm	55.71	50.9	8.5%

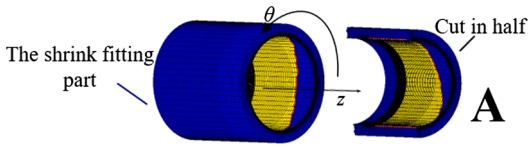

Fig. 8. Contact status along the shrink-fitted surface under the bending load w

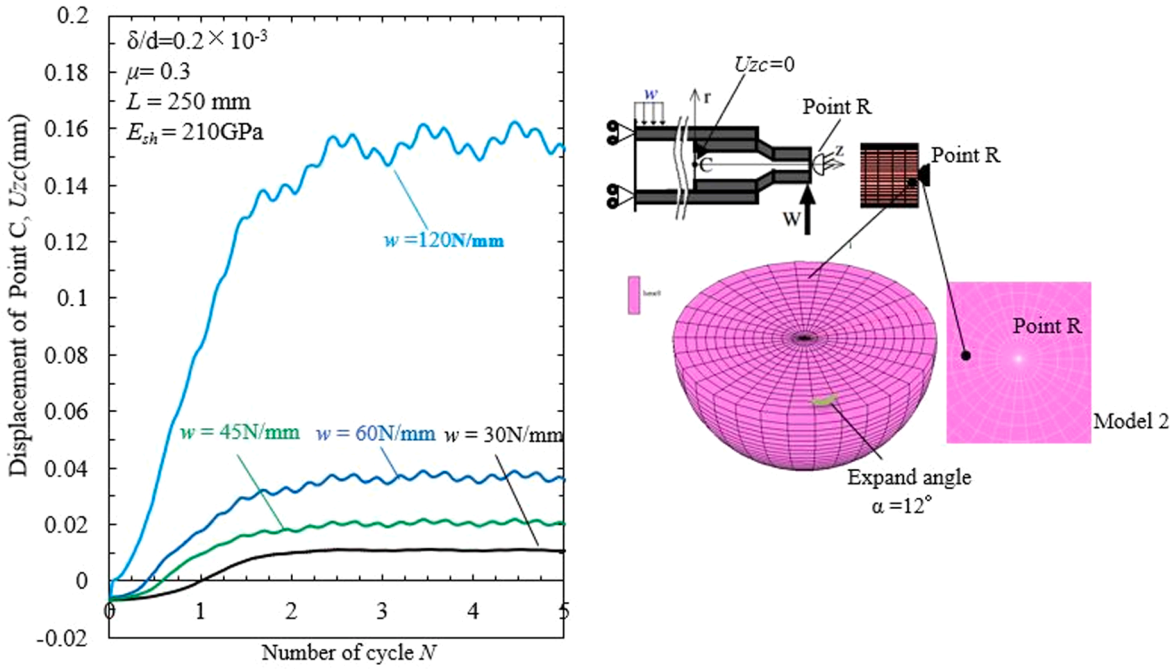

Fig. 9. Coming out displacement U_{zc} at point C vs loading cycles N when w = 30, 45, 60, 120 N/mm under fixed μ = 0.3, δ/d = 0.2 × 10^{-3}, L = 250 mm, E_{sh} = 210GPa

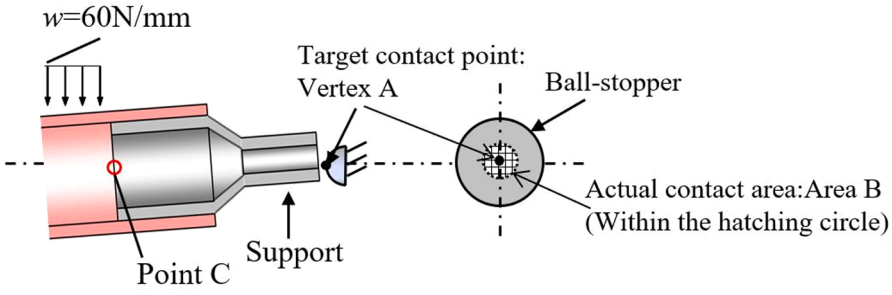

Fig. 10. Schematic illustration of the actual contact area B on the ball-stopper under shift loading status

3D model with a ball-stopper is newly introduced with the detailed dimensions in Fig. 4 to obtain the driving out force accurately. Fig. 5(d) shows the FEM mesh with the boundary conditions. Table 1 shows the mechanical properties of the modelling. The sleeve material is silicon nitride and the shaft is made of alloy steel. To obtain the contact force as F_d^{3D}, the ball-stopper is set as rigid, and the right end of the shaft structure is set as solid rigid elements rather than hollow. It should be noted that this study focuses on clarifying the phenomenon through the driving out force. The model in Fig. 5 (c) is suitable for identifying the driving out force. After clarifying the phenomenon, the real stopper can be designed in further studies to prevent the coming out. For this purpose, something similar geometry of the model in Fig. 5 (b) might be more suitable than the model in Fig. 5 (c).

In this study, the finite element method software MSC. Marc/Mentat 2012 with full Newton-Raphson iterative sparse solver of the

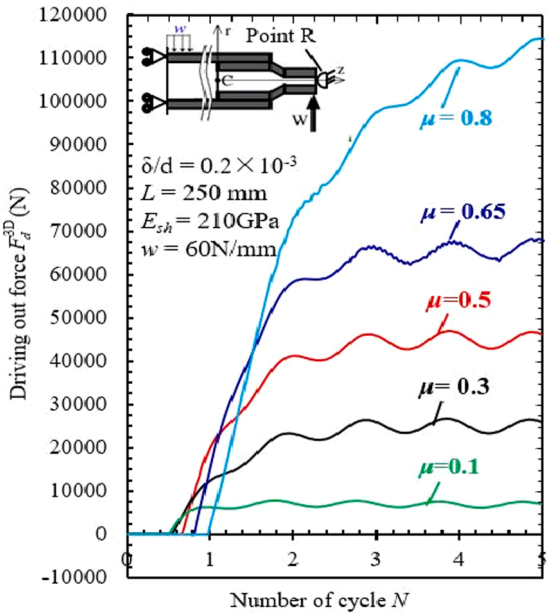

Fig. 11. Driving out force F_d^{3D} *vs* loading cycles N when the friction coefficients $\mu = 0.1, 0.3, 0.5, 0.65, 0.8$ under fixed $\delta/d = 0.2 \times 10^{-3}$, $w = 60$ N/mm, $L = 250$ mm, $E_{sh} = 210$GPa

Table 3
Driving out force F_d^{3D} and the frictional shear force $F_\tau^{resultant}$ at $N = 3.9$ where F_d^{3D} becomes stable at the peak position when the friction coefficients $\mu = 0.1, 0.3, 0.5, 0.65, 0.8$ under fixed $\delta/d = 0.2 \times 10^{-3}$, $w = 60$ N/mm, $L = 250$ mm, $E_{sh} = 210$GPa.

Friction coefficient μ	F_d^{3D} [kN]	$F_\tau^{resultant}$ [kN]	Error
0.1	7.67	7.07	8.0%
0.3	26.3	24.8	5.9%
0.5	46.7	42.9	8.2%
0.65	67.7	65.2	3.7%
0.8	107.1	101.3	5.4%

multi-frontal method is used [31]. The friction model has to be specified in the contact analysis. It is known that the Coulomb friction model can be widely used for most practical applications except for bulk-forming as encountered in e.g. forging processes although the arctangent model, stick–slip model, and bilinear model are available [32]. However, the arctangent model is unsuitable for estimating the typical relative sliding velocity prior when the sliding velocity varies largely during the analysis. Also, the stick–slip model needs a large amount of data to be determined from the repetitive calculation process [32]. In this paper, therefore, to avoid the huge computation time, the bilinear model is applied since the friction force is simply determined from the displacement [33].

Since the inertial force effect during the roller rotation can be neglected as shown in the previous paper [13], the quasi-static simulation can be performed by applying the load shifting method [13] as is shown in Fig. 6. In this method, the roll rotation is replaced by discrete load shifting with a load shift angle θ_0. In the previous paper, the shift angle θ_0 is changed from 6° to 12°, 18°, and 30° to select a proper value. Then, it is found that the coming out displacement at point C can be obtained with less than 1% error when $\theta_0 \leq 12°$ [13,19]. As the standard simulation conditions, the followings are used; the load $w = 30$ N/mm, shrink fitting ratio $\delta/d = 0.2 \times 10^{-3}$, the friction coefficient $\mu = 0.3$.

4. Identification of the driving out force F_d^{3D}

By using the model in Fig. 5 **(c), (d)**, after the steel shaft is coming out gradually from the sleeve, the shaft contacts with the ball-stopper. Then, the contact force F_s is generated. Obviously, the reaction F_s can be regarded as the driving out force F_d^{3D}. The reaction F_s has the same magnitude and acts in the opposite direction of F_d^{3D} as can be expressed in Eq. (1).

$$\left|F_d^{3D}\right| = |F_s| \tag{1}$$

The contact force can be obtained easily since only the vertex of the hemisphere ball-stopper in Fig. 5 **(c), (d)** contacts with the shaft. Since the contact force F_s is acting in the coming out z-direction, the driving out force F_d^{3D} can be obtained from Eq. (1).

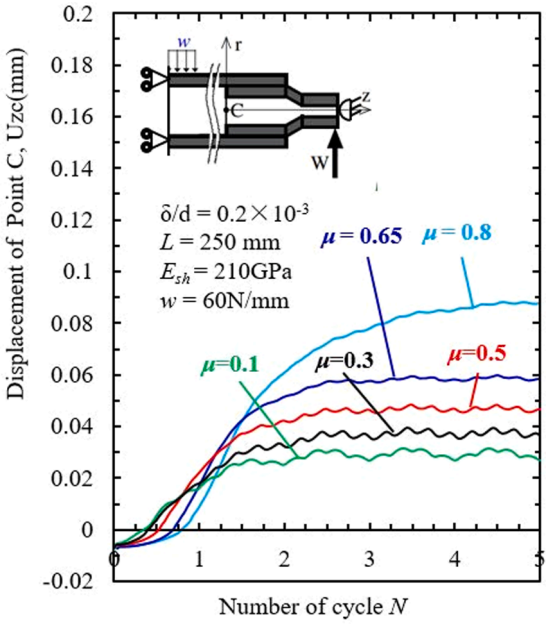

Fig. 12. Coming out displacement U_{zc} at point C vs loading cycles N when the friction coefficients $\mu = 0.1, 0.3, 0.5, 0.65, 0.8$ under fixed $\delta/d = 0.2 \times 10^{-3}$, $w = 60$ N/mm, $L = 250$ mm, $E_{sh} = 210$GPa

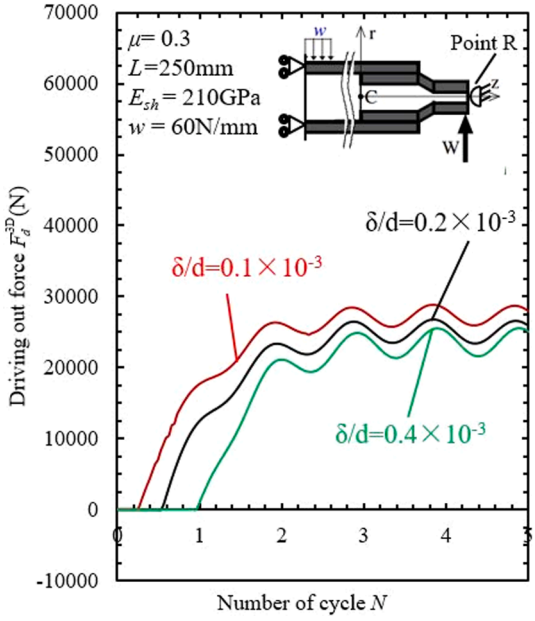

Fig. 13. Driving out force F_d^{3D} vs loading cycles N when the shrink fitting ratio $\delta/d = 0.1 \times 10^{-3}, 0.2 \times 10^{-3}, 0.4 \times 10^{-3}$ under fixed $\mu = 0.3$, $w = 60$ N/mm, $L = 150$ mm, $E_{sh} = 210$GPa.

Additionally, to understand why the driving our force F_d^{3D} appears, the frictional shear forces $F_\tau^{resultant}$ along the fitting portion between the shaft and sleeve under the load shifting should be calculated out. Then, confirm whether they satisfy Eq. (2) or not.

$$F_d^{3D} = F_\tau^{resultant} \tag{2}$$

Here, $F_\tau^{resultant}$ is the summation of the shear stress distributed along the inner cylinder surface. Since some inner portions are not in contact, the summation of all nodal forces at the contact portions is calculated to obtain $F_\tau^{resultant}$.

Fig. 7 shows the driving out force obtained from FEM model in Fig. 5(c), (d) by using ball-stopper 1 whose mesh angle $\alpha = 6°$ and

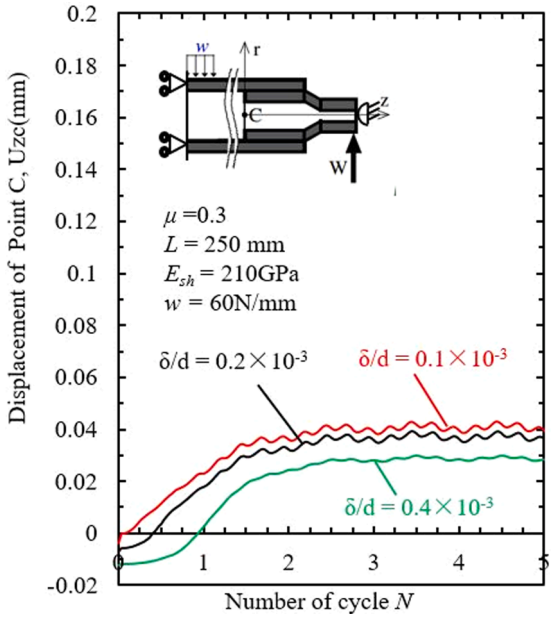

Fig. 14. Coming out displacement U_{zc} at point C vs loading cycles N when the shrink fitting ratio $\delta/d = 0.1 \times 10^{-3}$, 0.2×10^{-3}, 0.4×10^{-3} under fixed $\mu = 0.3$, $w = 60$ N/mm, $L = 150$ mm and $E_{sh} = 210$GPa.

Table 4
Driving out force F_d^{3D} and the frictional shear force $F_\tau^{resultant}$ at N = 3.9 where F_d^{3D} becomes relatively stable at the peak position when the shrink fitting ratios $\delta/d = 0.1 \times 10^{-3}$, 0.2×10^{-3}, 0.4×10^{-3} under fixed $\mu = 0.3$, $w = 60$ N/mm, $E_{sh} = 210$GPa.

Shrink fitting ratio δ/d	F_d^{3D} [kN]	$F_\tau^{resultant}$ [kN]	Error
0.1×10^{-3}	28.4	25.9	8.9%
0.2×10^{-3}	26.3	24.8	5.9%
0.4×10^{-3}	25.3	23.0	9.1%

ball-stopper 2 whose mesh angle $\alpha = 12°$. Since the difference is small between the two models, $\alpha = 12°$ is selected to save the calculation time. The driving out forces F_d^{3D} initially increase then become stable after 3 cycles due to the contact with the ball-stopper [30]. With increasing of the load magnitude, the peak values of F_d^{3D} increase.

Table 2 shows the driving out force F_d^{3D} in comparison with the frictional force $F_\tau^{resultant}$, which can be determined from

$$F_\tau^{resultant} = \int_A \tau_{\theta z} dA \tag{3}$$

where $\tau_{\theta z}$ is the frictional shear stress on the contact area A between the ceramic roller and the steel shaft illustrated in Fig. 8. As shown in Table 2, $F_\tau^{resultant}$ coincides with F_d^{3D} within 9 % error. The difference may be caused by the error of the numerical simulation. In the previous 2D modelling in Fig. 2(b) similar results can be seen [28–30].

Fig. 9 shows the coming out displacement U_{zc} at Point C obtained under the standard condition. The vibration can be seen in F_d^{3D} due to the discrete load shifting and the elastic deformations. As shown in Fig. 9, due to the shrink fitting of the ratio $\delta/d = 0.2 \times 10^{-3}$, the negative value of $U_{zc} = -0.007$ appears at N = 0. Such negative displacement due to the shrink fitting was illustrated previously [13]. Fig. 10 illustrates the contact area at the ball stopper. Instead of the target contact point Vertex A, the actual contact appears at Area B in Fig. 10. Similar to the variation of F_d^{3D} in Fig. 7, the coming out displacement U_{zc} at Point C increases at the beginning and becomes stable after several cycles. With increasing the load magnitude w, U_{zc} increases gradually when $w \leq 60$ N/mm, but U_{zc} increases much more significantly when $w \geq 60$ N/mm. Since the shaft comes out much more quickly, care should be taken for $w > 60$ N/mm. In Section 5, the fixed load magnitude $w = 60$ N/mm will be used as the standard load. To prevent the coming out failure, both of the driving out force F_d^{3D} and the coming out displacement U_{zc} per rotation can be reduced by decreasing the loading magnitude w.

5. Effects of fundamental design factors on the driving out force F_d^{3D} and the displacement U_{zc}

In the mechanical design of the sleeve roll, the most important factors can be the friction coefficients μ, shrink fitting ratios δ/d, shrink fitting length L, and the shaft Young's modulus E. Those effects on the driving out force F_d^{3D} and the displacement U_{zc} will be

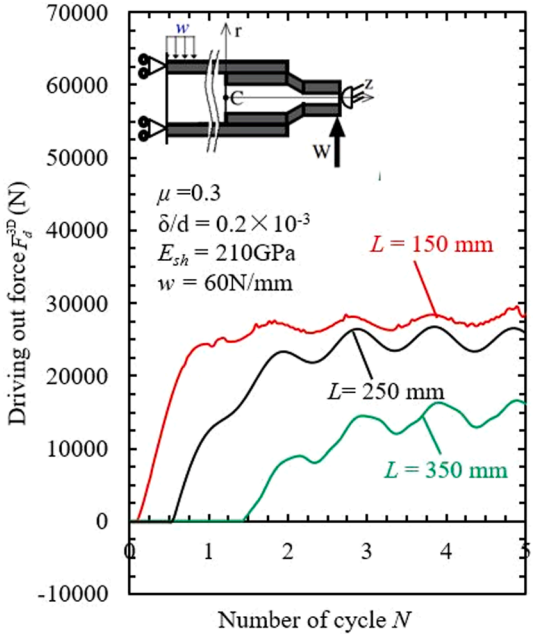

Fig. 15. Driving out force F_d^{3D} vs loading cycles N when the shrink fitting length L = 150, 250, 350 mm under fixed μ = 0.3, w = 60 N/mm, δ/d = 0.2 × 10^{-3}, E_{sh} = 210GPa.

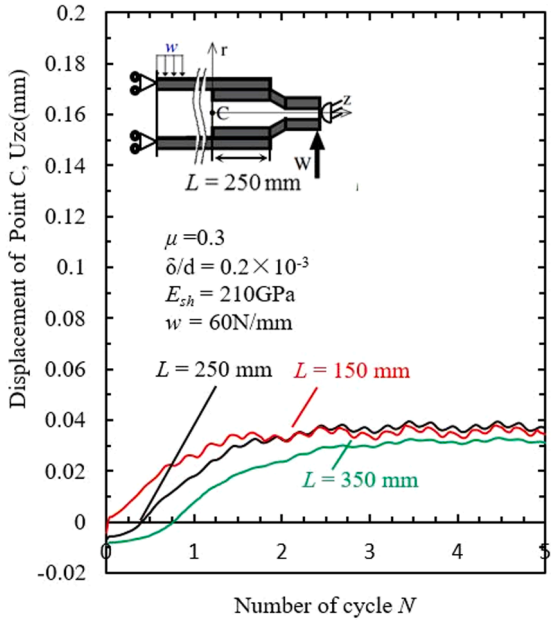

Fig. 16. Coming out displacement U_{zc} at point C vs loading cycles N when the shrink fitting length L = 150, 250, 350 mm under fixed μ = 0.3, w = 60 N/mm, δ/d = 0.2 × 10^{-3}, E_{sh} = 210GPa.

investigated in this Section. One may think how such fundamental design factors should be controlled toward avoiding the coming out phenomenon. However, the authors think this study should focus on clarifying the phenomenon. On the basis of the present results, the detailed design can be discussed in further studies to avoid the phenomenon.

5.1. *Effect of friction coefficient* μ

Fig. 11 shows the driving out force F_d^{3D} vs the loading cycle N by varying the friction coefficient μ in the range μ = 0.1 ~ 0.8 when

Table 5
Driving out force F_d^{3D} and the frictional shear force $F_\tau^{resultant}$ at $N = 3.9$ where F_d^{3D} becomes stable at the peak position when $L = 150$, 250, 350 mm under fixed $\mu = 0.3$, $w = 60$ N/mm, $\delta/d = 0.2 \times 10^{-3}$, $E_{sh} = 210$GPa.

L [mm]	F_d^{3D} [kN]	$F_\tau^{resultant}$ [kN]	Error
150	28.6	27.0	5.6%
250	26.3	24.8	5.9%
350	15.6	14.3	8.3%

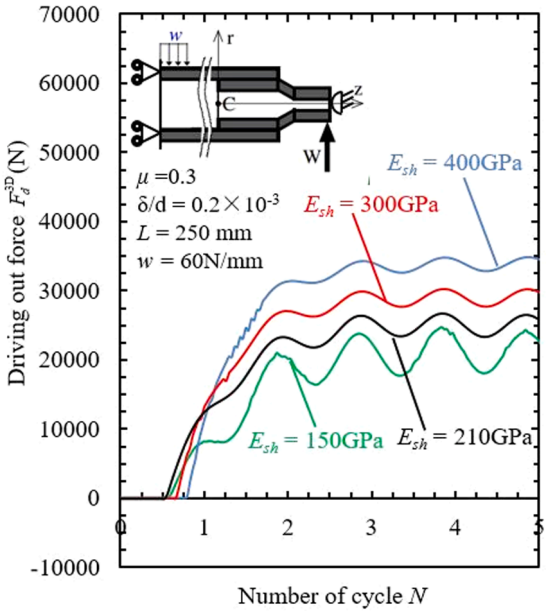

Fig. 17. Driving out force F_d^{3D} vs loading cycles N when the shaft Young's modulus $E_{sh} = 150$, 210, 300, 400GPa under fixed $\mu = 0.3$, $w = 60$ N/mm, $\delta/d = 0.2 \times 10^{-3}$, $L = 250$ mm

$\delta/d = 0.2 \times 10^{-3}$ and $w = 60$ N/mm. With increasing μ in the range $\mu = 0.1 \sim 0.8$, the driving out force F_d^{3D} increases. The range $\mu = 0 \sim 0.45$ is corresponding to the actual friction coefficient [34,35]. Table 3 shows the driving out force F_d^{3D} and the frictional force $F_\tau^{resultant}$ coincide with each other within 8.2 %error. Fig. 12 shows the coming out displacement per rotation U_{zc} vs the loading cycle N. The variation in Fig. 12 is similar to the variation in Fig. 11. Therefore, by decreasing the friction coefficient μ, both F_d^{3D} and U_{zc} can be reduced to prevent the coming out failure. However, if μ becomes $\mu = 0$, the axial frictional force against to the driving out force F_d^{3D} also becomes 0 and causing significant coming out failure. Therefore, the friction coefficient range $\mu = 0.1 \sim 0.3$ may be suitable. One may think how the friction coefficient can be reduced. In this study, however, to clarify the coming out phenomenon is mainly focused. After clarification, the details should be investigated to prevent the phenomenon in further studies, the authors think.

5.2. Effect of shrink fitting ratio δ/d

Fig. 13 shows F_d^{3D} vs the loading cycles N when the shrink fitting ratio $\delta/d = 0.1 \times 10^{-3} \sim 0.4 \times 10^{-3}$ under fixed load $P = 60$ N/mm and friction coefficient $\mu = 0.1$. When δ/d varies in the range $\delta/d = 0.1 \times 10^{-3} \sim 0.4 \times 10^{-3}$, F_d^{3D} varies in a similar way. Fig. 14 shows U_{zc} vs the loading cycles N. With increasing of δ/d,F_d^{3D} and U_{zc} decrease in a similar way. When δ/d varies in the range $\delta/d = 0.1 \times 10^{-3} \sim 0.4 \times 10^{-3}$, U_{zc} varies in a similar way. Table 4 shows the driving out force F_d^{3D} and the frictional force $F_\tau^{resultant}$ coincide with each other within 9.1 %. To prevent the coming out failure, Both of the driving out force F_d^{3D} and the coming out displacement U_{zc} per rotation can be reduced by increasing the shrink fitting ratio δ/d.

5.3. Effect of the shrink fitting length L

Fig. 15 shows the effect of the shrink fitting length L on F_d^{3D}. Fig. 16 shows the effect of the shrink fitting length L on U_{zc}. Table 5 shows F_d^{3D} and $F_\tau^{resultant}$ coincide with each other within 8.3 %. With increasing L, F_d^{3D} and U_{zc} decrease as shown in Fig. 15 and Fig. 16.

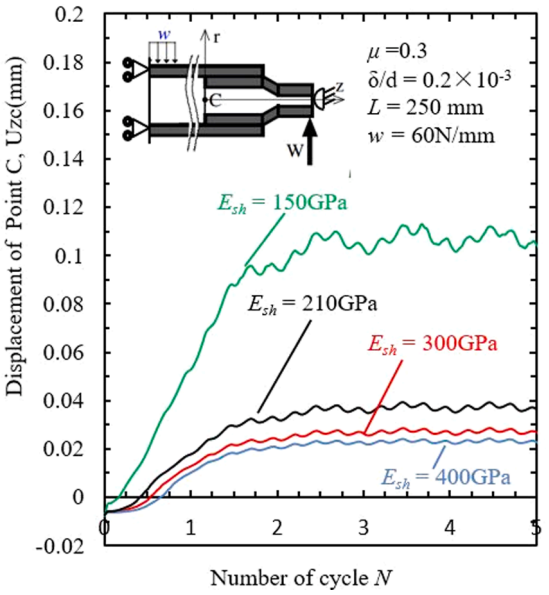

Fig. 18. Coming out displacement U_{zc} at point C vs loading cycles N when the shaft Young's modulus E_{sh} = 150, 210, 300, 400GPa under fixed μ = 0.3, w = 60 N/mm, δ/d = 0.2 × 10^{-3}, L = 250 mm

Table 6
Driving out force F_d^{3D} and the frictional shear force $F_\tau^{resultant}$ at N = 3.9 when F_d^{3D} becomes relatively stable at the peak position when the shaft Young's modulus E_{sh} = 150, 210, 300, 400GPa under fixed μ = 0.3, w = 60 N/mm, δ/d = 0.2 × 10^{-3}, L = 250 mm.

E_{sh} [GPa]	F_d^{3D} [kN]	$F_\tau^{resultant}$ [kN]	Error
150	25.1	24.3	3.2%
210	26.3	24.8	5.9%
300	30.5	28.9	5.2%
400	35.0	32.9	6%

With increasing L, the coming out displacement per rotation U_{zc} also decreases. Although a longer fitting length may prevent the shaft coming out, such length L = 350 mm is unsuitable because of the high cost [28 ~ 30]. Moreover, if the fitted portion L is longer, some portion has to be situated at the inside of a high-temperature furnace where very high temperature is applied. Therefore, the suitable fitted length can be in the range 150 < L *less than 350*. To prevent the coming out failure, both of the driving out force F_d^{3D} and the coming out displacement U_{zc} per rotation can be reduced by increasing the shrink fitting length L.

5.4. *Effect of Young's modulus E_{sh}*

In this Section, the shaft Young's Modulus E_{sh} is changed in the rangeE_{sh} = 150 ~ 400GPa to understand the coming out phenomena. Instead of the shaft coming out displacement in the z-direction focused in this study, the shaft slip displacement in the θ-direction was recently investigated for the sleeve roll used as a rolling roll [36]. The results showed that the θ-displacement increases by decreasing the shaft's elastic Young's Modulus E_{sh}. In other words, it was found that the shaft slip displacement is promoted by the shaft's elastic deformation.

Fig. 17 clarifies the effect of Young's Modulus E_{sh} on the driving out force F_d^{3D}. Fig. 18 clarifies the effect of the shaft Young's modulus E_{sh} on the coming out displacement U_{zc}. Table 6 shows F_d^{3D} and $F_\tau^{resultant}$ coincide with each other within 6 %. With decreasing E_{sh}, F_d^{3D} decrease as shown in Fig. 17 but U_{zc} increases as shown in Fig. 18. With decreasing E_{sh}, the elastic deformation becomes larger and the shaft movement becomes easier. Although similar tendency was reported for the circumferential slippage in sleeve rolling roll [36], Fig. 18 shows that U_{zc} is promoted more significantly by the elastic deformation of the shaft. As shown in Fig. 18, the displacement U_{zc} decreases with increasing the shaft Young's modulus E_{sh}; however, the diving out force F_d^{3D} increases with increasing E_{sh} as shown in Fig. 17. To prevent the coming out failure, by decreasing the shaft Young's modulus E_{sh}, the driving out force F_d^{3D} can be reduced although the coming out displacement U_{zc} per rotation increases.

6. Conclusions

Ceramics sleeve rolls have been developed to be used efficiently under high temperatures to produce high-quality steel plates in steel manufacturing industries. Since the shrink-fitted shafts are connected at both ends of the ceramic sleeve under only a small shrink-fitting ratio due to the ceramic brittleness, sometimes coming out of the shaft appears during the use although there is no external force applied in the coming out direction. This study focused on identifying the driving out force F_d^{3D} through a three-dimensional numerical simulation. As the most fundamental design factors, the effects of the friction coefficients, the shrink fitting ratios, the fitting length, and Young's modulus on F_d^{3D} were also discussed. Then, the conclusions can be summarized in the following way.

(1) The driving out force can be identified from the reaction force appearing at the ball stopper after the shaft is coming out and contacts with the stopper. It was found that the driving out force F_d^{3D} is generated as the summation of the frictional shear stress $F_\tau^{resultant}$ along the shrink-fitted cylindrical surface under the bending load w. The summation of the frictional shear forces $F_\tau^{resultant}$ coincides with the contact force F_d^{3D} within 3.2 ~ 9.1% error.

(2) During the early stage of the contact between the stopper and the shaft, the driving out force F_d^{3D} increases, then becomes stable and nearly constant after several loading cycles due to the stopping work of the ball-stopper. A similar tendency can be seen for the coming out displacement at the shaft end.

(3) The driving out force F_d^{3D} is found to be in the range of $F_d^{3D} = 26.3\text{kN} \sim 35\text{kN}$ when the frictional coefficient $\mu = 0.3$, the shrink fitting ratio $\delta/d = 0.1 \times 10^{-3} \sim \delta/d = 0.4 \times 10^{-3}$, the fitting portion length $L = 150 \sim 350$ mm, and the shaft Young's modulus $E_{sh} = 150 \sim 400$GPa.

(4) The driving out force F_d^{3D} increases significantly with increasing the friction coefficient μ (see Fig. 11). Although when $\mu = 0.3 \sim 0.5$ the driving out force $F_d^{3D} = 26.3 \sim 46.7$kN, when $\mu = 0.8$, the driving out force becomes $F_d^{3D} = 107.1$kN. With increasing μ, the coming out displacement U_{zc} also increases (see Fig. 12).

(5) The effects of the fundamental design factors are also clarified to prevent coming out failure. Both of the driving out force F_d^{3D} and the coming out displacement U_{zc} can be reduced by decreasing the loading magnitude w (see Fig. 7) and the friction coefficient μ (see Fig. 11, Fig. 12). Also, both of F_d^{3D} and U_{zc} can be reduced by increasing the shrink fitting ratio δ/d (see Fig. 13, Fig. 14) and the shrink fitting length L (see Fig. 15, Fig. 16). By decreasing the shaft Young's modulus E_{sh} (see Fig. 17, Fig. 18), the driving out force F_d^{3D} can be reduced although the coming out displacement U_{zc} increases.

Declaration of Competing Interest

The authors declare that they have no known competing financial interests or personal relationships that could have appeared to influence the work reported in this paper.

References

[1] S. Hamayoshi, E. Ogawa, K. Shimizu, N.A Noda, K. Kishi, S.Koga, Development of Large Ceramic Rolls for Continuous Hot Dipping Steel Sheet Production Line. Sokeizai, 51, (2010), 54-58(in Japanese).
[2] N.A. Noda, Y. Sano, Y. Takase, W. Li, H. Sakai, Application of Large Ceramics Structures to Steel Manufacturing Machinery, Int. J. Eng. Innov. Manag. 1 (2011) 77–82.
[3] E. Ogawa et al., Practical Evaluation of Large Ceramic Rolls for Continuous Hot Dipping Steel Sheet Production Line, Hitachi Met. Tech. Rev., 28(2012), 50-55 (in Japanese).
[4] W. Li, H. Sakai, S. Harada, Y. Takase, N.-A. Noda, Y. Sano, Yoshikazu Sano, Thermal Stress During Separation for Ceramics Sleeve and Shaft Connected by Shrink Fitting, J. S. Mech. Materials Engineering 6 (4) (2012) 251–264, https://doi.org/10.1299/jmmp.6.251.
[5] R. P. Larsen, A. D. Vyas, The outlook for ceramics in heat engines, SAE Tech. Paper No. 1988-02-085514 (1988).
[6] P. Wray, Advanced Structural Ceramics, Tech Monitoring, SRI Int, Japan, 1991.
[7] S. Jahanmir, Friction and Wear of Ceramics, Marcell Dekker, New York, 1994.
[8] U. Dworak, High-tech Ceramics "Viewpoints and perspectives", K. Gernot, Academic Press Limited, London, 1989.
[9] M. Fujii, A. Yoshida, J. Ishimaru, S. Shigemura, K. Tani, Influence of Sprayed Layer Thickness on Rolling Contact Fatigue of Ceramics Sprayed Roller, Trans. Jpn. Soc. Mech. Eng. C, 72(2006), 1354. (In Japanese). https://doi.org/10.1299/kikaic.72.1354.
[10] C. Liour, T. Mori, H. Kobayashi, T. Mitamura, Mitamura, Influence of Various Atmospheres on the Corrosion Resistance of Si3N4 Sintered Bodies against Steel Making Slag and Its Main Components, JCS-Japan, 98(1990), 348 -354 (in Japanese). https://doi.org/10.2109/jcersj.98.348.
[11] T. Ono, Current status and future prospect of the development of high performance ceramics, J. Jpn. Soc, Mech. Eng. 86 (1983) 470–475, https://doi.org/10.1299/jsmemag.86.774_470, in Japanese.
[12] S. Sen, B. Aksakal, Stress analysis of interference fitted shaft–hub system under transient heat transfer conditions, Mate. Design 25 (5) (2004) 407–417, https://doi.org/10.1016/j.matdes.2003.11.009.
[13] N.A. Noda, D. Suryadi, S. Kumasaki, Y. Sano, Y. Takase, Failure analysis for coming out of shaft from shrink-fitted ceramic sleeve, Eng. Fail. Anal. 57 (2015) 219–235, https://doi.org/10.1016/j.engfailanal.2015.07.016.
[14] N.-A. Noda, Y. Xu, D. Suryadi, Y. Sano, Y. Takase, Coming Out Mechanism of Steel Shaft from Ceramic Sleeve, ISIJ Int. 56 (2) (2016) 303–310.
[15] E. Ogawa, K. Shimizu, S. Hamayoshi, N. Kumagai, Y. Ohtsubo, N.A. Noda, Y. Takase, K. Kishi, K. Shobu, T. Tabaru, E. Maeda, S. Koga, T. Matsuda, Practical evaluation of large ceramic rolls for continuous hot dipping steel sheet production line, Hitachi Met. Tech. Re. 28 (2012) 50–55. In Japanese.
[16] M. Tsuyunaru, N.A. Noda, Hendra, Y. Takase, Maximum Stress for Shrink Fitting System Used for Ceramics Conveying Rollers, Trans. Jpn. Soc. Mech. Eng. A, 74 (2008), 919-925.
[17] A. Rusin, G. Nowak, W. Piecha, Shrink connection modelling of the steam turbine rotor, Eng. Fail. Anal. 34 (2013) 217–227, https://doi.org/10.1016/j.engfailanal.2013.08.002.

[18] S. Matsuda, D. Suryadi, N.A. Noda, Y. Sano, Y. Takase, S. Harada. Structural design for ceramics rollers used in the heating furnace, Trans. Jpn. Soc. Mech. Eng. A, 79(2013), 989-999. https://doi.org/10.1299/kikaia.79.989.
[19] N.-A. Noda, D. Suryadi, S. Matsuda, Y. Sano, Y. Takase, Proposal for new hearth roller consisting of ceramic sleeve and steel shafts used in the heat treat furnace, ISIJ Int. 55 (11) (2015) 2416–2425, https://doi.org/10.2355/isijinternational.ISIJINT-2015-246.
[20] N.-A. Noda, Y. Takase, M. Tsuyunaru, Maximum Stress for Shrink Fitting System Used for Ceramics Conveying Rollers, JMMP 2 (11) (2008) 1410–1419.
[21] N.-A. Noda, M. Yamada, Y. Sano, S. Sugiyama, S. Kobayashi, Thermal stress for all-ceramics rolls used in molten metal to produce stable high quality galvanized steel sheets, Eng. Fail. Anal. 15 (4) (2008) 261–274, https://doi.org/10.1016/j.engfailanal.2007.03.003.
[22] N.A. Noda, Hendra, M. Oosato, K. Suzumoto, Y. Takase, W. Li. Strength analysis for shrink fitting system used for ceramics rolls in the continuous pickling line, Key Eng. Material. 462-463(2011), 1140-1145. https://doi.org/10.4028/www.scientific.net/KEM.462-463.1140.
[23] W. Li, N.-A. Noda, H. Sakai, Y. Takase, Analysis of Separation Conditions for Shrink Fitting System Used for Ceramics Conveying Rollers, Journal of Solid Mechanics and Materials, Engineering 5 (1) (2011) 14–24, https://doi.org/10.1299/jmmp.5.14.
[24] W. Li, N.A. Noda, H. Sakai, Y. Takase, Thermal stress analysis for shrink fitting system used for ceramics conveying rollers in the process of separation, Key. Eng. Material 452–453 (2011) 241–244, https://doi.org/10.4028/www.scientific.net/KEM.452-453.241.
[25] C.E. Truman, J.D. Booker, Analysis of a shrink-fit failure on a gear hub/shaft assembly, Eng. Fail. Anal. 14 (4) (2007) 557–572, https://doi.org/10.1016/j.engfailanal.2006.03.008.
[26] N. Antoni, Contact separation and failure analysis of a rotating thermo-elastoplastic shrink-fit assembly, Appl. Math. Model. 37 (4) (2013) 2352–2363, https://doi.org/10.1016/j.apm.2012.05.018.
[27] J. Zhao, J.X. Wang, C. Yu, S.Q. Tang, J. Yao, Influence of radial interference on torque capacity of shrink-fit camshaft, Adv. Mech. Eng. 2019, 11(4). https://doi.org/10.1177/1687814018817640.
[28] G.W. Zhang, H. Sakai, N.A. Noda, Y. Sano, S. Oshiro, Generation Mechanism of Driving Out Force of the Shaft from the Shrink Fitted Ceramic Roll by Introducing Newly Designed Stopper, ISIJ Int. 59 (2) (2019) 293–299, https://doi.org/10.2355/isijinternational. ISIJINT-2018-615.
[29] G.W. Zhang, Mechanism clarification of coming out of the shaft from shrink-fitted ceramic sleeve roller under bending load focusing on the driving-out force, Ph.D. Thesis, Department of Mechanical and Control Engineering, Kyushu Institute of Technology, Kitakyushu, Japan (2020).
[30] N.A. Noda, G.W. Zhang, Y. Sano, H. Sakai, Y. Takase, Effects of design factors on the driving-out force of the steel shaft in a shrink-fitted ceramic roller, J. Mech. Sci. Technol. 35 (4) (2021) 1559–1568, https://doi.org/10.1007/s12206-021-0320-y.
[31] Marc Mentat team, Theory and User Information. Vol. A, MSC.Software. Tokyo, 713-722, 2012.
[32] Marc Mentat team, Theory and User Information. Vol. A, MSC.Software. Tokyo, 545-561, 2012.
[33] Marc Mentat team, Theory and User Information. Vol. A, MSC.Software. Tokyo, 572-595, 2012.
[34] X.Z. Zhao, J.J. Liu, B.L. Zhu, H.Z. Miao, Z.B. Luo, Friction and Wear of Si3N4 Ceramic/Stainless Steel Sliding Contacts in Dry and Lubricated Conditions, J. Mater. Eng. Perform. 6 (2) (1997) 203–208, https://doi.org/10.1007/s11665-997-0015-2.
[35] K.-H. Zum Gahr, Sliding wear of ceramic-ceramic, ceramic-steel and steel-steel pairs in lubricated and unlubricated contact, Wear 133 (1) (1989) 1–22, https://doi.org/10.1016/0043-1648(89)90109-9.
[36] N.-A. Noda, R. Abdul Rafar, H. Sakai, X. Zheng, H. Tsurumaru, Y. Sano, Y. Takase, Irreversible interfacial slip in shrink-fitted bimetallic work roll promoted by roll deformation, Eng. Fail. Anal 126 (2021) 105465, https://doi.org/10.1016/j.engfailanal.2021.105465.